Astron. Astrophys. 233, 82–95 (1990)

ASTRONOMY
AND
ASTROPHYSICS

Box and peanut shapes generated by stellar bars

F. Combes[1,2], **F. Debbasch**[1,2], **D. Friedli**[3], **and D. Pfenniger**[3]

[1] Observatoire de Meudon, F–92190 Meudon, France
[2] Ecole Normale Supérieure, F–75005 Paris, France
[3] Observatoire de Genève, CH–1290 Sauverny, Switzerland

Received December 4, 1989; accepted February 12, 1990

Abstract. By means of three-dimensional N-body simulations, we find that all the stellar bars that develop in realistic models of collisionless disk galaxies take after some time a more or less pronounced peanut-shape when seen edge-on. According to the projection direction, the bar can also appear box-shaped or round. This morphology gradually appears after the bar has formed and reaches its maximum intensity when the bar is in a steady state; there is then a wide resonance zone corresponding to a marginal horizontal Inner Lindblad Resonance (ILR) ($\Omega_b = \Omega - \kappa/2$), and a distinct vertical ILR ($\Omega_b = \Omega - \nu_z/2$). Stars in this zone oscillate along orbits far from the plane, forming the peanut shape. The mechanism is estimated to be efficient enough to account for all edge-on spiral galaxies that are observed box- or peanut-shaped. However, the boxy shapes in ellipticals are probably of different nature.

Key words: kinematics and dynamics of galaxies – structure of galaxies – barred galaxies

1. Introduction

For a long time, edge-on disk galaxies have revealed peculiar structures such as box or peanut shapes in their center (Burbidge & Burbidge, 1959; galaxies NGC 128 and NGC 7332, page 7 of Hubble Atlas, Sandage, 1961). Recently this phenomenon has received much attention, both from an observational point of view (Jarvis, 1986; Shaw, 1987, 1989; de Souza & dos Anjos, 1987; Dettmar, 1989), and from theoretical investigations (Binney & Petrou, 1985; May et al., 1985; Pfenniger, 1985; Petrou, 1987; Rowley, 1988; Bailey & Wilkinson, 1990). This attention is raised in a large part by the aim to understand the dynamical structure of spheroidal components. Now that elliptical galaxies have been recognized not to be simple oblate systems supported by rotation (cf. Binney, 1982), the structure of bulges of disk galaxies, that have long been assimilated to the elliptical family, is gaining special interest, as a clue to the origin of the whole family of spheroids.

Boxy isophotes have also been observed in elliptical galaxies (Lauer, 1985ab; Jedrzejewski, 1987): about one third of all ellipticals are box-shaped, while only one third reveal perfect ellipses as isophotes (cf. Nieto, 1988). The hope is that such distortions are the relics of the galaxy formation, while an ellipsoidal system is what is expected after relaxation, when all initial conditions have been washed out. For instance, Binney & Petrou (1985) suggest that the deformation is the remnant of a merger; this idea is attractive since it can be assimilated to the proposition that all the ellipticals have been built from successive violent mergers (e.g. Toomre, 1977; Schweizer, 1986).

However, there seem to be qualitative differences between bulges and ellipticals, as far as these deformations are concerned: the tendency to box shapes is much more pronounced in bulges than in ellipticals, and peanut shapes are never observed in ellipticals. Box and peanut bulges are characterised by cylindrical rotation, and not spheroidal rotation (Jarvis, 1987, 1990; Kormendy & Illingworth, 1982)[1] Also, according to Jensen & Thuan (1982), the box-shaped bulge of NGC 4565 at least displays an exponential light distribution rather than the $r^{1/4}$ law.

In the present paper, we are only concerned by the box and peanut shapes occurring in disk galaxies, since boxy isophotes in ellipticals seem to be a quantitatively (and might be qualitatively) different phenomenon. Up to now, essentially four different processes have been proposed to explain the box and peanut shapes as well as the associated cylindrical rotation:

1) External torques. May et al. (1985) constructed a self-consistent N-body model of a box-shaped bulge through the action of an external cylindrically symmetric torque on a spheroidal stable system. However, such a torque, being an ad-hoc experimental device, is problematical to relate to some astrophysical counterpart, even in an early phase of galaxy formation. The main interest of this work is to show that cylindrical box-shaped galaxies belong to the set of feasible self-gravitating systems.

2) Dissipational mechanism. Bailey & Wilkinson (1990) suggested that dynamical friction on molecular clouds in the disk could transfer angular momentum into the bulge, which would then enhance the rotation of stars with large vertical oscillations. In some way, this mechanism provides the torque assumed in 1).

Send offprint requests to: D. Pfenniger

[1] The rapid cylindrical rotation and the stellar disk in the unusually strong box-shaped elliptical galaxy IC 3370 lead Jarvis (1987) to reclassify it as a S0pec.

However such a process has difficulties to produce the observed amount of boxiness, especially in early type galaxies.

3) Cannibalism or "soft-merging". Binney & Petrou (1985) constructed a stellar distribution function involving a heavily populated peculiar family of orbits (2-D subset) with respect to all possible orbits (3-D continuum in action space), in order to obtain a box-shaped model out of a rotating spheroidal one. They suggested that such a model could result either from a merger between two disk galaxies with favourable orientation, or by accretion of material from satellites. Whitmore & Bell (1988) argued that the accretion of material from a companion could produce either a polar-ring galaxy (impact at a right angle to the disk) or a box- or peanut-shaped galaxy (impact at an oblique angle). However, the 41 box- or peanut-shaped galaxies discussed in Jarvis (1986), and the 74 in de Souza & dos Anjos (1987) do not show much evidence for significant merging or tidal interaction (as debris, shells, loops, or tidal deformations). Shaw (1987, 1989) finds also that the environment of box-shaped galaxies is quite comparable to that of a control sample: peanut galaxies are not more interacting than ordinary galaxies. Also, from the theoretical point of view, it remains to be shown that the assumed axisymmetry is not destroyed after the merging of a substantial amount of mass rotating at a high speed. Indeed, the fraction of mass in the bulge of a typical peanut galaxy is often important; in IC 4767, Whitmore & Bell (1988) mention that "the amount of mass in the X-component is about the same as the mass in the disk".

4) Bars. In a previous paper, Combes & Sanders (1981) (CS), have shown with the help of 3-D N-body simulations of disk systems, that the stellar bars formed in the disks revealed precisely box and peanut shapes when viewed edge-on. More specifically, bars are peanut-shaped when the line of sight is edge-on, round when end-on, and box-shaped when intermediate. These structures were then proposed to be formed by a resonance phenomenon, between the rotating motion of the bar, and perpendicular oscillations of the stars. When resonant, stars would gain energy from the bar, and see their z-oscillation amplitude increased. This resonance occurs inside the bar region (i.e. inside the corotation radius). Other previous 3-D simulations of bar leading to box or peanut shapes can be found in the works of Hohl & Zang (1979) and Miller & Smith (1979), though these authors did not point out the possible link with box-shaped bulges. Pfenniger (1984) developed this hypothesis in his 3-D dynamical study of barred galaxies: he determined the stability properties of the main families of periodic orbits, and found that the strength and axis ratios of the bar were constrained by horizontal as well as vertical instabilities. The strength of the vertical instabilities inside a bar, *especially inside a flat one*, is such that inevitably at some locations orbits have to leave rapidly the galactic plane. In particular, he found a family of stable periodic orbits that could trap stars above the plane and have a box shape. This was further explored in Pfenniger (1985), where chaotic motion associated with the general vertical instability offers a way to redistribute matter into the bulge by semi-ergodic diffusion. We remark that the observations of several typical box-shaped galaxies (NGC 1381, Carvalho & da Costa, 1987; NGC 5170, Dettmar & Barteldrees, 1988) or peanut-shaped galaxies (the SBab NGC 2654 and the SB0 NGC 4469, Jarvis, 1986) reveal the presence of bars.

In order to determine which of the above interpretations applies to which objects, further simulations and observations are clearly necessary. But, keeping in mind that the majority of disk galaxies have observed non-axisymmetric central regions, the relations between bars and bulges can not be simply ignored, as done by the scenarios 1), 2) and 3). In this paper we want to examine in more detail the nature and formation mechanisms of these peculiar shapes in barred galaxies. First, we will confirm the very presence and frequent appearance of these shapes in self-gravitating galaxy disks developing a bar, by more accurate and different N-body codes, and by varied initial conditions. In particular, we wrote new 3-D codes with variable spatial resolution across the galaxy, in order to increase the resolution at the center and the dynamical range, and to better eliminate numerical artifacts. Second, we want to determine the necessary conditions in the potential for these structures to appear. We performed simulations with two initial components (bulge and disk), tried different mass distributions (involving parameters such as the bulge-to-disk mass ratio), and chose the distribution of the velocity dispersion either in hydrostatic equilibrium or by fixing the Q parameter (Toomre, 1964). Finally, the results can be interpreted as consequence of a resonance between vertical oscillations and the bar pattern speed (in particular we observe a vertical inner Lindblad resonance). The shape of the underlying orbits is also briefly discussed. Subsequent papers will address the problem from the general point of view of dynamical systems (Debbasch & Combes, 1990), including studies of periodic orbits and bifurcations (Pfenniger & Friedli, 1990).

2. Models and methods

We have carried out a series of 3-D N-body simulations, for studying the conditions of appearance and the frequency of box and peanut shapes. In order to firmly establish the fidelity of our results, independently of the numerical treatment, the simulations have been done by means of different codes, developed and run separately in Geneva and Paris on different computer types.

2.1. Units

For convenience, we set G to 1, the mass unit to $2 \cdot 10^{11} M_{\odot}$, the length unit to 1 kpc, which imply a time unit of $1.05 \cdot 10^{6}$ yr, and a velocity unit of $930\,\mathrm{km\,s^{-1}}$. Below we call dynamical time (T_{dyn}) 100 time units ($\approx 10^{8}$ yr), which corresponds about to the period of the orbits making the peanut shapes described below, and half the bar rotation period.

2.2. Codes specifications

The codes are all based on the Particle-Mesh (PM) method, on the Fast Fourier Transforms (FFT) technique to solve Poisson's equation. Indeed, this technique is presently still the most efficient for simulating quiet disks at a given resolution and number of particles (Sellwood, 1987). The assignment of mass to grid points and the interpolation between grid points for determining forces are calculated through the Cloud-In-Cell (CIC) scheme (Hockney & Eastwood, 1981). The grids have cartesian or polar geometry and, for the latter, different laws for the spacing in the radial direction.

Table 1. Codes characteristics

code	N_R	N_ϕ	N_z	$R_{\max}$	R_f	h_z	ϵ	ΔT
CAR	256	256	128	16	0.25	0.12	0.5	1.0
P3	24	36	120	41	0.03	0.13	1.0	1.0
PE1	24	36	120	56	0.20	0.13	1.0	1.0
PE2	31	32	125	100	0.10	0.20	$\epsilon(R)$	0.5

code: type of code (see Sect. 2.2).
N_R: number of radial cells (or N_x for CAR).
N_ϕ: number of azimuthal cells (or N_y for CAR).
N_z: number of vertical cells.
$R_{\max}$: radial maximum grid dimension (in kpc).
R_f: first radial cell size (in kpc).
h_z: vertical cell spacing (in kpc).
ϵ: softening length (in kpc).
ΔT: time-step ($\approx$ in million years).

Our main goal being to discuss the box and peanut structure, and the general method being well tested and documented in the literature, we only describe succinctly the codes. More detailed considerations of our codes are delayed to more technical papers.

The different codes can be separated in four classes:

1) Code with a cartesian grid (CAR). This code has been described previously (cf. CS).

2) Code with a polar grid and a R^3 power-law spacing (P3). These polar codes are extensions to 3-D of the polar N-body code described by Miller (1976, 1978), and also by Sellwood (1981). The grid points in the $z=0$ plane are distributed on N_ϕ radial spokes (separated by equal angles of $360/N_\phi$ degrees), at the intersections with N_R centered rings. The rings are non-uniformly distributed in radii but in a R^3 power-law (following the larger concentration of stars towards the center) with the first ring at R_f and an extension up to $R_{\max}$. In the z-direction, the grid is linear, containing N_z cells with a constant spacing h_z. However, to avoid the interaction with images, the galaxy is confined in z on half the cell numbers ($N_z/2$). This problem does not exist in the $x-y$ plane, where the natural periodicity in ϕ allows to work on all N_ϕ cells. Contrary to 2-D, in 3-D the potential is no longer a convolution of the density with respect to a radial variable, thus the potential is not computed by FFT, but by direct summations. Since N_R does not need to be very large in order to reach an acceptable resolution in the center, the processing time required for solving Poisson's integral remains comparable with the time to move forward the particles. Contrary to the codes of Miller or Sellwood, the central hole is suppressed and we treat this region as normal grid cells[2]. In the $z=0$ plane for instance, the central mesh point is the center of a cell where all quantities are averaged over the angle ϕ. A pile of such cells surrounds the z-axis. Particles are then moved forward normally through the central cylinder. The radial grid lines being non-parallel, a radial self-force on each particle remains. This self-force is directly calculated and subtracted from each particle at each time-step. In this way, a single isolated particle moves on a straight line. The softening length ϵ equals 2–3 R_f; but ϵ being smaller than the cells in the outer parts, the potential is there softened by the grid itself. Particles are moved forward by using Buneman's algorithm (1967).

[2] In 3-D, a central empty column of cells would have disastrous dynamical effects.

3) Code with a polar grid and an exponential spacing (PE1). The same as 2) except that the radial spacing is exponential.

4) Code with a polar grid, an exponential spacing and a cell size dependent softening (PE2). Besides the different values of the typical parameters (see Table 1), this code differs from 3) by a non-constant softening length ϵ, that varies accordingly to the cell size, from $\epsilon = 0.2$ at the center, to $\epsilon = 0.66$ at $R = 3$, to $\epsilon = 1.9$ at $R = 10$. This has been found to decrease the amplification of the spatial high frequencies. The self-forces are pre-computed and stored in a table, and found by interpolation during the simulation. The time integration scheme is a time-centered leap-frog with a constant time-step ΔT, chosen such that particles do not cross more than one cell per time-step (see Pfenniger & Friedli, 1990). Some typical code specifications are listed in Table 1.

2.3. Initial conditions

Our aim being to study the long term evolution of bars, the simplest way to build a self-consistent model of bar is to start from slightly unstable axisymmetric disks, which are known to rapidly develop a bar. All the initial equilibrium galaxy models are built with two components: a disk and a bulge. The disk is represented by self-gravitating particles, and the bulge is either rigid, represented by a Plummer potential, or consists of self-gravitating particles. The comparison between the two sets of simulations gives some insight into the interaction between the bulge and disk components. The total number of particles is N and the simulations are performed over fairly long time scales, typically between 20 up to 200 dynamical times $T_{\rm dyn}$.

The initial mass distribution of the disks has been chosen from two models, differing essentially in the third dimension.

Component of type $\mathscr{T}$. The particles are initially distributed in a Kuzmin disk (Kuzmin, 1956), with a surface density $\mu(R) = \mu_0(1+R^2/A_d^2)^{-3/2}$. Next, the disk is thickened in the z-direction by a $\mathrm{sech}^2(z/H_d)$ function, the isothermal infinite plane distribution. The initial dependence of the plane height $H_d(R)$ with R follows the law $H_d(R) = H_d(0)\sqrt{1-R^2/R_d^2}$, where R_d is the maximum radius of the initial disk.

Component of type $\mathscr{M}$. The particle distribution follows the Miyamoto model (Miyamoto & Nagai, 1975; Nagai & Miyamoto, 1976), which is inspired by a Kuzmin disk in the $x-y$ plane, but where the z-distribution of particles is such that the resulting potential $\Phi_{\rm MN}$ has the form:

$$\Phi_{\rm MN}(R,z) = -\frac{GM_d}{\sqrt{R^2+\left(A_d+\sqrt{H_d^2+z^2}\right)^2}}, \qquad (1)$$

where M_d is the disk mass, H_d a characteristic thickness, and $A_d + H_d$ a radial scale-length.

The initial mass distribution of the bulges has the same formal shape as the Miyamoto disks, the index d being replaced by b. Usually the radial scale $A_b + H_b$ is comparable with H_d (A_b is a small positive quantity). If $A_b = 0$, $\Phi_{\rm MN}$ is a Plummer potential (*component of type $\mathscr{P}$*).

Table 2. Characteristics of some runs

run	code	type	q	α	β	γ	Q	N	T_{tot}
A	CAR	$\mathscr{P}+\mathscr{T}$	0.50		0.25	0.16	0.8	4	30.0
B	CAR	$\mathscr{M}+\mathscr{M}$	1.00	0.25	0.20	0.20	$Q(R)$	4	42.5
C	CAR	$\mathscr{M}+\mathscr{M}$	1.00	0.25	0.10	0.10	$Q(R)$	4	42.5
D*	CAR	$\mathscr{M}+\mathscr{M}$	1.00	0.25	0.20	0.20	$Q(R)$	4	42.5
E	CAR	$\mathscr{M}+\mathscr{M}$	1.00	0.50	0.20	0.20	$Q(R)$	4	42.5
F	P3	$\mathscr{P}+\mathscr{M}$	1.00		0.50	0.16	$Q(R)$	2	200.0
G+	P3	$\mathscr{P}+\mathscr{T}$	2.00		0.25	0.08	0.5	2	160.0
H	PE1	$\mathscr{P}+\mathscr{T}$	0.50		0.25	0.08	0.8	2	20.0
I	PE1	$\mathscr{P}+\mathscr{T}$	1.00		0.25	0.08	0.8	2	20.0
J+	PE1	$\mathscr{P}+\mathscr{T}$	2.00		0.25	0.08	0.8	2	22.0
K	PE1	$\mathscr{P}+\mathscr{T}$	0.50		0.25	0.08	0.4	2	20.0
L	PE1	$\mathscr{P}+\mathscr{T}$	1.00		0.25	0.08	0.4	2	20.0
M	PE1	$\mathscr{M}+\mathscr{M}$	1.00	0.25	0.20	0.20	$Q(R)$	4	42.5
N	PE2	$\mathscr{M}+\mathscr{M}$	0.18	0.05	0.33	0.33	$Q(R)$	20	60.0
O	PE2	$\mathscr{P}+\mathscr{M}$	0.05		0.08	0.08	$Q(R)$	20	20.0

code: type of code (see Sect. 2.2).
type: type of initial conditions (see Sect. 2.3).
q: bulge to disk mass ratio M_b/M_d.
length ratios: $\alpha=A_b/A_d$, $\beta=H_b/A_d$, $\gamma=H_d/A_d$.
Q: initial value of the Toomre parameter.
N: number of particles (in ten thousand).
T_{tot}: simulation duration in T_{dyn} (in $\approx 10^8$yr).
*: run with a softening length of 1 kpc.
+: no bar found.

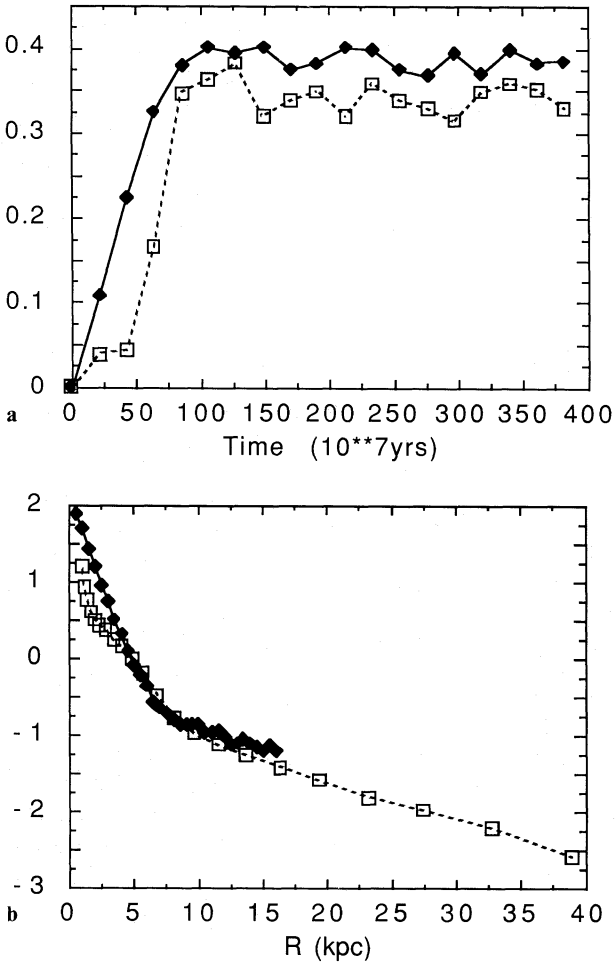

Fig. 1. Comparison between simulations made from the same initial conditions with the two grids: polar (open squares, run M) and cartesian (filled diamonds, run D). (a) strength of the bar Q_2 as a function of time; (b) radial surface density, when the bar has reached a quasi steady-state ($T=20\,T_{dyn}\approx 2\cdot 10^9$ yr).

In the case of two Miyamoto components with the same vertical scale heights ($H_b = H_d$) and for an isotropic velocity dispersion, solutions of the stellar hydrodynamical equations for the mean rotational velocity V_ϕ and for the velocity dispersion σ exist in closed form (Nagai & Miyamoto, 1976). However, strictly consistent solutions do not exist for every values of the parameters. In order to get a real velocity V_ϕ everywhere, especially around the center, A_b has to be greater than some minimum value $A_{b\,\min}$. Nevertheless, runs were sometimes performed with $A_b < A_{b\,\min}$ (e.g. $A_b = 0$); then V_ϕ has been set to zero, and, for preserving the virial ratio for each layer at constant z, the velocity dispersion σ has been decreased by the corresponding amount.

In the case of a thickened Kuzmin disk and a Plummer bulge, the potential must be determined with the help of the N-body integrator itself in order to calculate subsequent quantities for the disk such as the rotational velocity V_{rot} and the epicyclic frequency κ. The radial velocity dispersion σ_R may be chosen such as to correspond to the minimum value ensuring axisymmetric stability i.e. $\sigma_R/\sigma_{R\,crit} = Q = 1$, where $\sigma_{R\,crit} = 3.36G\mu/\kappa$ (Toomre, 1964). Lower values of Q were also used, since the presence of a softening stabilises against such instabilities. In particular a cold initial disk ($Q = 0$) has been computed in presence of a massive bulge (see CS). These calculations were used to launch particles in the Plummer component in a non-rotating isotropic distribution. The same procedure can be used in the case of two Miyamoto components but with different scale heights $H_b \neq H_d$.

The main free parameters that were varied are the mass-ratio between the bulge and the disk $q = M_b/M_d$, the concentration ratio (mainly the ratio $\alpha = A_b/A_d$), and the vertical scale-heights (ratio $\beta = H_b/A_d$ and $\gamma = H_d/A_d$).

A couple of models have also been started in slight non-equilibrium, by decreasing the particle velocities by a few percents. Such models quickly reajust and subsequently evolve as the initially equilibrium models.

Up to now, more than 100 runs were performed with different grids, different initial conditions, and different machines, from a MicroVax II up to a Cray-2. But, for the sake of brevity, we only list here the detailed characteristics of representative runs from which the figures of this article has been issued. They are named and described in Table 2. The whole data set was of course used to find the general trends and results described in Sect. 3.

2.4. Tests

Numerous tests were performed, such as the check that a single particle moves on a straight line, or that the potential of a single particle is indeed precisely Keplerian outside its softening radius. The conservation of total energy and angular momentum were verified at the 0.3% and 0.02% level respectively per T_{dyn}, the discrepancy coming essentially from the particles which escape

from the grid. In the stable models (with a high bulge/disk ratio), before the apparition of the bar, the energy conservation was much better, of order of that of the angular momentum (almost no escaped particles).

We have verified that these figures are independent of the time-step ΔT ($100 \leq \Delta T/T_{\rm dyn} \leq 400$), the number of particles ($2 \cdot 10^4 \leq N \leq 5 \cdot 10^5$), the 32 or 64 bit arithmetic, as well as the computer architecture (Alliant FX/1, Cray-2, Vax, IBM 3090).

3. Simulations

3.1. Comparison between polar and cartesian grids

Results between the two methods are in a general good agreement. The strengths of the bars, as measured by Q_2 (see next Section), are comparable (Fig. 1a), although somewhat higher with the cartesian grid. This is easily accounted for by the larger softening of the polar grid. Indeed, the softening length ϵ has been chosen equal to 1 kpc in the two runs, but the cell size becomes larger in the outer parts for the polar grid. Also, we can notice a larger slope in the central concentration of particles in polar-grid models, and especially when the bar instability has multiplied the number of elongated orbits. At the same evolution time, the same galaxies are less centrally bright with the cartesian method (Fig. 1b).

This can obviously result from the different cell-sizes in the center. The cartesian grid smooths out the possible central gradient, that can develop better in the thinner polar grid. This effect is small in view of the small difference in absolute cell-size, in particular in the $256 \cdot 256 \cdot 128$ grid (where the resolution is of order of 0.25 kpc, for a galaxy mass of $10^{11}\,M_\odot$).

3.2. Bar instability

In most of our simulations, a bar instability, that we are looking for, develops, and remains almost unchanged until the end, which corresponds up to a Hubble time. Characteristic trailing bisymmetric spiral arms accompany the formation of the bar, and transport angular momentum outwards, as in numerous earlier 2- and 3-D simulations (e.g. Hohl, 1971). The transient spiral waves take some angular momentum away, and slow down the central stars.

When the bar settles down, it always rotates with a high velocity. With time, more and more particles are trapped by the bar, which extends farther in radius: its corotation radius moves somewhat outwards, and the bar slightly slows down. The e-decay time of the bar rotation speed amounts typically to about $50\,T_{\rm dyn}$, in no case as fast as predicted by Weinberg (1985), a few $T_{\rm dyn}$. The ratio of the bar semi-major axis to the corotation radius always remains of order of one. Of course, the exact value of this ratio depends on the bar length definition.

The variation of the bulge to disk mass ratio allows us to vary essentially the strength of the bar formed: indeed as was already shown (CS), the bar instability occurs sooner and with a larger strength when the M_b/M_d ratio is smaller. Figure 2 shows the bar strength, estimated from the maximum ratio Q_2 between the second order tangential force and the radial force; if the total potential in the $z=0$ plane is developed in Fourier series:

$$\Phi(R,\phi) = \Phi_0(R) + \sum_{m=1} \Phi_{2m}(R) \cos 2m(\phi - \phi_0) \qquad (2)$$

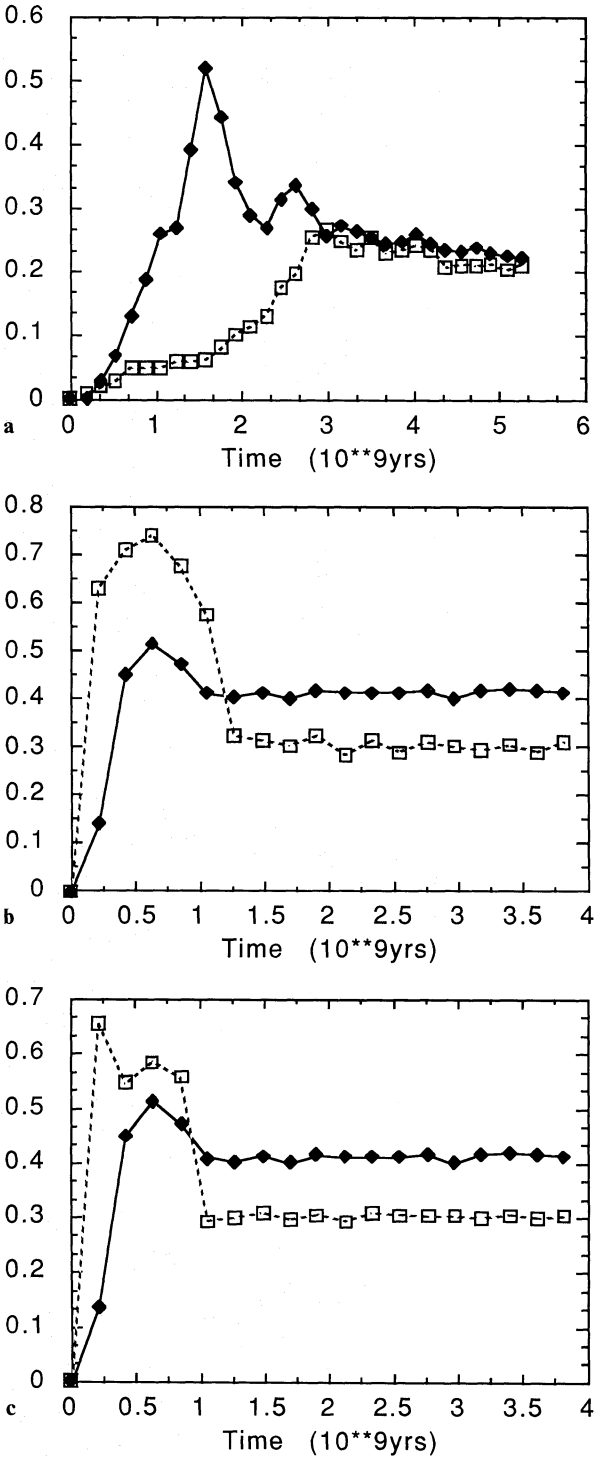

Fig. 2a,b,c. Comparison of the bar growth for various runs. (a) influence of the bulge to disk mass ratio $q=M_b/M_d$ (filled diamonds, run H, open squares, run I); (b) influence of the bulge-to-disk scale ratio $\alpha=A_b/A_d$ (filled diamonds, run B, open squares, run E); (c) influence of the scale height (filled diamonds, run B, open squares, run C).

then $Q_{2m}(R)$ is defined as

$$Q_{2m}(R) = 2m\,\Phi_{2m}(R) \Big/ R\,\frac{\partial \Phi_0}{\partial R}(R). \qquad (3)$$

Our high resolution allows us to confirm previous results; the

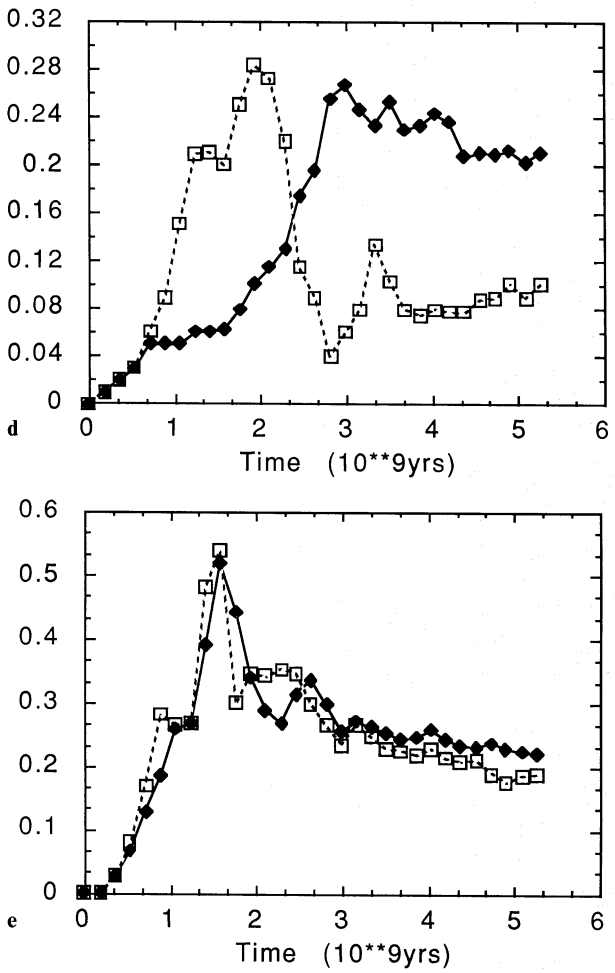

Fig. 2d,e. (d) influence of the initial amount of velocity dispersion (parameter Q) (filled diamonds, run I, open squares, run L); (e) the same, but for a lower bulge to disk mass ratio (filled diamonds, run H, open squares, run K). When the initial velocity dispersion is so low as to confer a large instability to the system, the consequent heating is such that the system becomes then more stable than with a larger initial Q; that explains these two diagrams.

growing times of the bar instability are comparable to those found by CS, taking into account the lower number of particles (noisier initial state), the larger softening length (by at least a factor 2), and the colder system at the beginning that were used. The main differences are noticed for very unstable systems (low M_b/M_d), where the influence of initial conditions is more important. When the system has had time to relax to an equilibrium state, the difference is not significant (case $M_b/M_d=2$ for instance).

All our disks with a ratio M_b/M_d at least equal to 2, and possessing some velocity dispersion initially were stable on scales of order of the Hubble time (for instance run J and G in Table 2).

We have also tested the influence of varying the amount of velocity dispersion with radius across the galaxy. A disk similar to that of run A, possessing initially a ratio $Q=3$ in the inner parts, while keeping $Q=1$ in the external parts, was indeed much more stable against bar-formation. The bar instability was delayed at least until 20 $T_{\rm dyn}$ ($\approx 2\cdot 10^9$ yr), and we did not pursue such simulations.

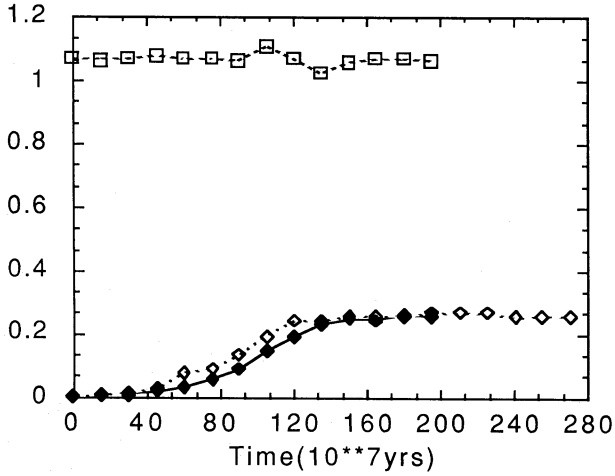

Fig. 3. Influence of the disk on a self-gravitating and non-rotating bulge. The particles are distributed in a Plummer sphere with an isotropic velocity distribution. The evolution of the strength of the bar (Q_2) is represented for run A (open diamonds) and its analog, but with a "live" Plummer (filled diamonds). For this latter run the bulge axis-ratio b/a is also plotted (open squares), computed directly on the particles by quadratic means of coordinates (The flattening of the bulge is hardly detected, i.e. $b/a \approx 1$).

3.3. Influence of the disk evolution on the bulge

The group of particles distributed in the bulge component at the beginning of the simulation was followed to investigate its sensitivity to the disk gravity.

If the bulge is initially non-rotating, its evolution is very slow, and during many revolutions, little interaction between the bulge and disk components occurs. This can be attributed to the high velocity dispersion in the bulge, and to the limited thickness of the disk. In particular, no significant flattening of the bulge-particles distribution has been measured, and also the radial distribution was stable. The test is shown for experiment A, for a mass ratio of $M_b/M_d=0.5$ (Fig. 3). This behaviour was already noticed by Sellwood (1980), who then justified the use of rigid representations of bulges in N-body simulations.

The situation changes in the case of a rotating bulge. If the bulge is consistent with the hydrodynamical equations, it rotates somewhat and may exchange angular momentum with the disk. Usually the converse of the non-rotating case is observed, the rotating bulge looses a fraction of its angular momentum as the bar develops, because it participates also to the bar instability. In many cases, the bulge tends to be prolate with its major axis aligned with the one of the bar.

Though the hot component is hardly modified by the disk evolution, the apparent bulge component can be enriched by disk stars. This phenomenon is difficult to quantify, but is striking in the case of a simulation with no initial bulge ($M_b=0$): we observe in projection a thickening of the disk plane, in the regions where the bar develops, which, depending on the point of view, can be mistaken with a "bulge". This remarkable thickening of the disk corresponds to the peanut phenomenon.

3.4. When does the box-peanut shape appear?

The peanut qualifier is used here as soon as the projected density contour lines along the rotation axis are concave. The

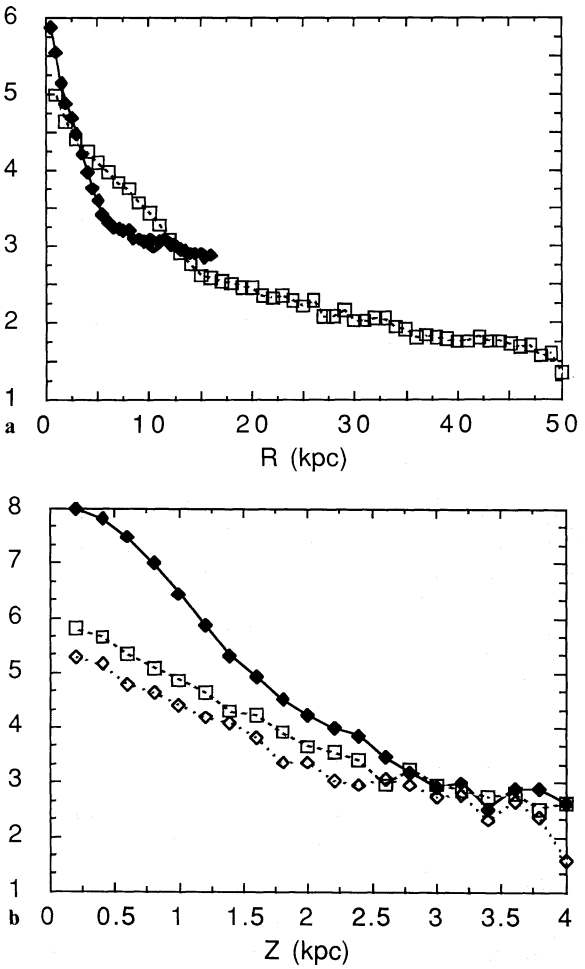

Fig. 4. Equilibrium projected density distribution: (a) in the radial direction, (run C at $T = 30\,T_{\rm dyn} \approx 3 \cdot 10^9$ yr, filled diamonds, and run F at $T = 200\,T_{\rm dyn} \approx 20 \cdot 10^9$ yr, open squares). The polar grid model (F) extends much farther out than the cartesian grid one (C). The projected density is exponential over large distances, but presents two characteristic radial-scales. (b) perpendicular to the galactic plane (run C at $T = 30\,T_{\rm dyn} \approx 3 \cdot 10^9$ yr, at different radii R ($R = 1$, filled diamonds, $R = 2$, open squares, $R = 3$, open diamonds). The projected density is approximately exponential.

box qualifier is used for straight or slightly convex contour lines. In no case, in the observations as well as in the models, do the *isophotes* or density contours have a X-shape, as described by Whitmore and Bell (1988), since the isophotes along the galactic plane are never concave.

After a sufficiently long time, as soon as a relatively strong bar has formed, the box or peanut shape has been produced in a few dynamical times *without exception*. This does not depend for instance on the initial thickness of the disk, or the initial z-velocity dispersion, or the z-density profile. In fact, the violent relaxation that occurs in the first time-steps washes out initial conditions quickly: the final radial-law of the surface density of the disk tends towards an exponential, whatever the initial conditions are (Fig. 4a). The final z-law of the scale height of the disk tends approximately towards an exponential (Fig. 4b). The models where the disk was initially unrealistically thin, with corresponding low z-velocity dispersion, give rise also to a peanut-shape, but with a lower scale-height. When a hot bulge is present, the peanut-shape is made of stars initially in the disk. Therefore, if the stars of both the disk and the bulge are projected simultaneously, the more massive is the bulge, the less peanut-shaped is the total model. In this way, systems with different degrees of boxiness can be built.

In order to quantify the box-peanut distortions, we measure the coefficient a_4 as used by observers on elliptical galaxies (Bender and Möllenhoff, 1987). We determine this from the shape of isophotes of the density in the $x-z$ projection, Ox being along the major axis of the bar. We choose the isophote of maximum departure from an ellipse. This isophote is first rectified to the second order by a homothetic transformation in z (axis ratio of the best-fitted ellipse), and its departure from a circle then yields the a_4 Fourier coefficient,

$$\Delta r = a_4 \langle r \rangle \cos 4\theta. \tag{4}$$

The value of a_4 is negative for a box- or peanut-shaped $x-z$ profile, but positive for a diamond- or disk-shaped profile. Therefore, at the beginning of the run the value $a_4(0)$ is positive. Then, we define the box-peanut strength as the departure from this initial value, i.e.,

$$P_4(T) = a_4(0) - a_4(T). \tag{5}$$

The time of appearance of the peanut shape is somewhat delayed with respect to the time of appearance of the bar (Fig. 5a). We interpret this by the fact that the width and strength of vertical resonances in the ($z = 0$) plane increase with *the horizontal and vertical eccentricity* of the bar (Pfenniger, 1984). Once a strong bar has formed, several revolutions are necessary for the disk to thicken in projection and saturate the instabilities. This delay is not a constant, since several parameters are involved in determining the bar strength, such as the M_b/M_d ratio, the mass concentration, and the initial temperature distribution. For example, a set of models (with one component of type $\mathscr{M}$, e.g. $q = 0$), which differ at start only by the flattening ($\gamma = 1/2$, $1/3$ and $1/4$), leads to bars with nearly the same horizontal density axis-ratio. The density axis-ratio is first related to the initial flattening of the model, but then a general thickening occurs; the flatter the model is initially, the more important is the resulting thickening (about 8%, 56% and 77% respectively). At $T = 40\,T_{\rm dyn}$, the vertical bar axis-ratio is then comparable for the three models, but the shape of the isophotes differ when seen edge-on: round for $\gamma = 1/2$, boxy for $\gamma = 1/3$ and peanut-shaped for $\gamma = 1/4$.

The position of the maximum elevation in the peanut-shape slowly drifts radially outwards. This evolution is displayed in Fig. 5b, where we have reported the radius of the maximum z of the $x-z$ density isophotes. This phenomenon is linked to the slowing down of the bar, since stars making up the peanut are resonant with the bar (see Sect. 3.7, 3.8 and 3.9).

3.5. Morphology of the peanut

The projected density contour lines were examined for various orientations of the galaxy, showing the observable morphology in dependence on the view angles. For the projections, we use a spherical coordinate system in agreement with the one often used in astronomy, so the inclination angle has a different convention that the one often used in physics. In a $x-y-z$ coordinate system, the rotation axis lies along the z-axis. In the $x-y$ plane

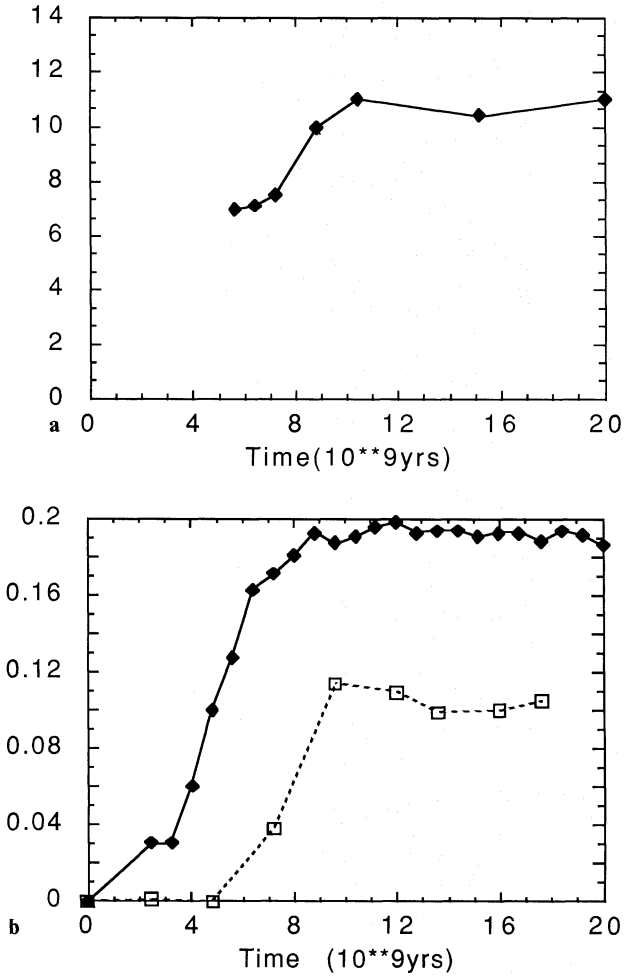

Fig. 5. (a) Evidence of a time delay between the apparition of the bar, and that of the peanut indicated by the bar strength parameter Q_2 (diamonds) and the peanut strength parameter P_4 (squares) in run F. (b) Radius of the maximum elevation of the peanut, as a function of time (run F).

the major and minor axes of the bar are along the x and y axes respectively. The azimuth (longitude) ϕ starts along the major axis of the bar. The inclination (latitude) θ starts in the galactic plane. A face-on view corresponds to the inclination $\theta=90°$, an edge-on view to $\theta=0°$, $\phi=90°$, and an end-on view corresponds to $\theta=0°$, $\phi=0°$.

We show the appearance of a well developed box-peanut galaxy with a small initial bulge ($q=0.05$) in projection on the plane of the sky (Fig. 6, left): face-on the bar has already a rectangular shape. A heavier and hotter bulge would make the bar shape rounder in the center. When the disk is edge-on, the box-peanut morphology is observed whenever the angle between the line of sight and the bar major axis is larger than 30°. As the disk is inclined from edge-on, the box-peanut morphology gradually passes to the face-on aspect. Among the galaxies with an inclination angle θ less than 10°, the subjective percentage of favourable projection angle has been estimated to be 50% for a peanut, and 35% for a box-shape (bar almost along the line of sight). Renormalising these values to 0.85 (the fraction of favorable projections to see box or peanut), the predicted ratio between observed peanuts and boxes amounts then to about 58%, while the observed one is about 60% (Jarvis, 1986; Shaw, 1987, 1989; de Souza and dos Anjos, 1987; Dettmar, 1989). However, since a precise definition of box or peanut shapes is still lacking, the above figures for our models as well as for actual galaxies should be considered as approximate and indicative.

3.6. Kinematics

As for the density, we have projected the principal observable kinematical quantities of several models at different stages of evolution, along different lines of sight, that is, the density weighted projected radial velocity $V_{\rm rad}$ and the projected radial velocity dispersion $\sigma_{\rm rad}$ (Fig. 6, middle and right).

In the literature (e.g. Bertola & Capaccioli, 1977; Kormendy & Illingworth, 1982) peanut- and box-shaped galaxies are associated with an almost cylindrical rotation, though this schematic description is based on a few examples. One has to consider that the observed cylindrical rotations in galaxies are limited to the brightest part of the galaxies, because at increasing z the measurements are rapidly very noisy and time consuming. On the other hand, from dynamical arguments, one can expect that at *some* height, rotation has to decrease, the precise turnover height being still unknown. In the models, we find quite clearly that the cylindrical rotation is confined to the inner, brightest parts. When seen end-on, no particular morphological signs reveals the presence of a peanut or a bar, the models look just like typical edge-on galaxies with an exponential disk and a nearly round (but bright) bulge. The kinematics only reveals some differences. When $\theta=0°$ and especially for an edge-on view ($\phi=90°$), the $V_{\rm rad}$ contour lines exhibit a rotation which is more cylindrical than the initial model (at $T=0$), but extending only 2–3 kpc above the ($z=0$) plane, and about 3 kpc in R, while the peanut ends at about $R=5$ kpc. For model N, in the edge-on projection at $R=3$ kpc and $z=3$ kpc, the velocity decreasing with respect to $z=0$ kpc amounts to: at $T=1\,T_{\rm dyn}$ (no peanut, no bar), 78 km/s, at $T=12\,T_{\rm dyn}$ (no peanut, but a well developed bar), 40 km/s, and at $T=40\,T_{\rm dyn}$ (peanut and bar well developed), 25 km/s (Fig. 7). An observational test for the detection of a bar in edge-on galaxies could be the presence of a rotation near the center which would be more cylindrical than would be expected from a spheroidal system.

At any angle, the contour lines of the velocity dispersion $\sigma_{\rm rad}$ are rounder than the ones of the density. The higher values are present at the center and decrease with increasing R or z. The velocity dispersion $\sigma_{\rm rad}$ is the largest when the bar is seen end-on. When $\theta=90°$, $\sigma_{\rm rad}$ corresponds to the projected velocity dispersion in z and the contour lines deviate only slightly from circularity.

At intermediate angles, the velocity field (Fig. 6, middle) has a clear distortion, which is less the case for the velocity dispersion field (Fig. 6, right).

3.7. Peanut and axisymmetric resonances

Approximate locations of resonances due to the bar can be obtained by averaging the potential in azimuth. Then the horizontal and vertical epicyclic frequencies κ and ν_z can be compared easily with the circular orbit frequency Ω and the pattern speed of the bar Ω_b, giving the radii of resonances. These frequencies have a precise meaning only in the axisymmetric case, and the averaging in azimuth does not inform us about non-linearities introduced by the important bar deformation. Therefore, one has to check

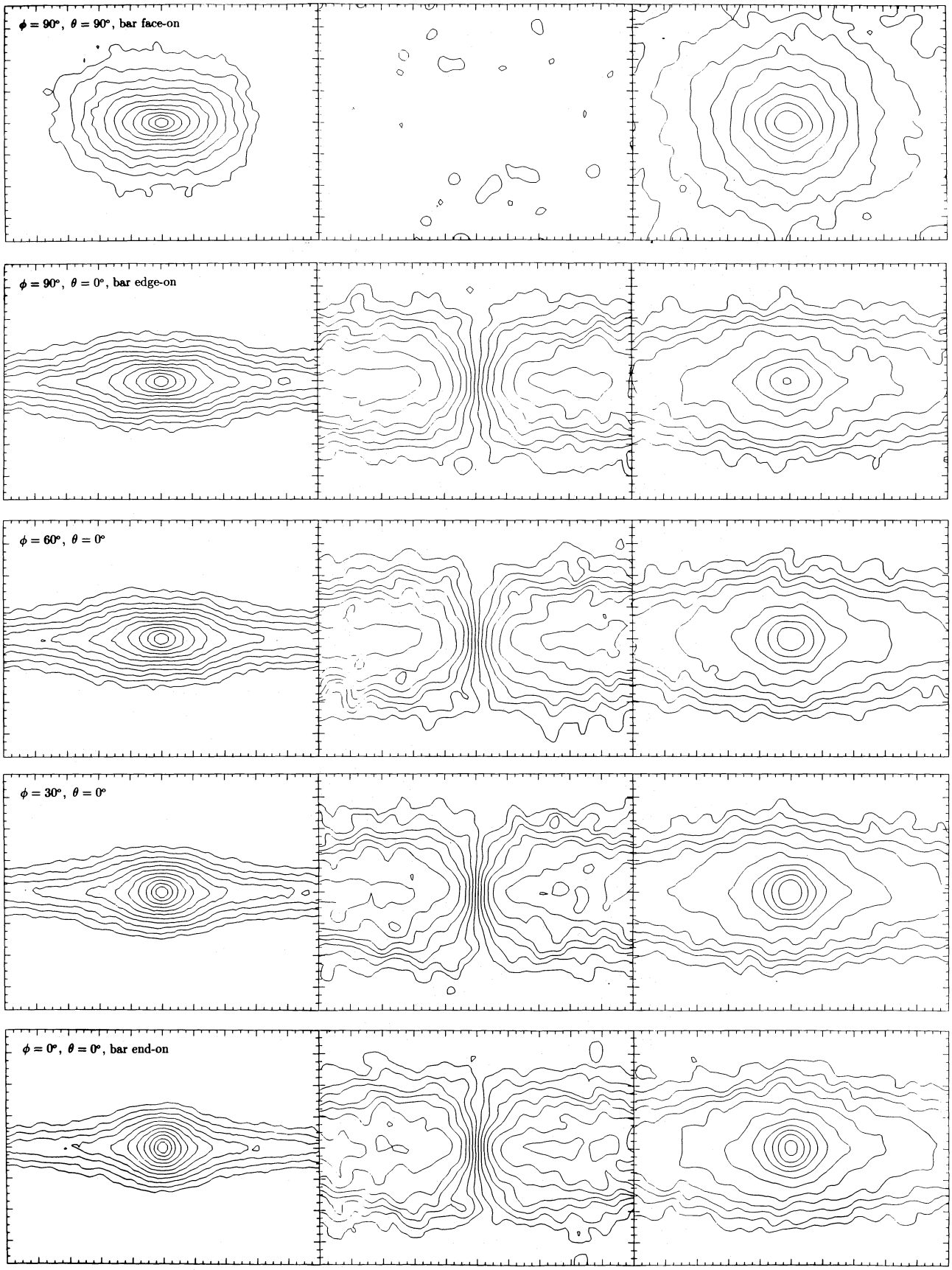

Fig. 6. Projections at different angles of the density (left), the radial velocity (middle), and the velocity dispersion (right) (run O at $T = 20\,T_{\rm dyn}$). The definitions of the viewing angles are given in Sect. 3.5

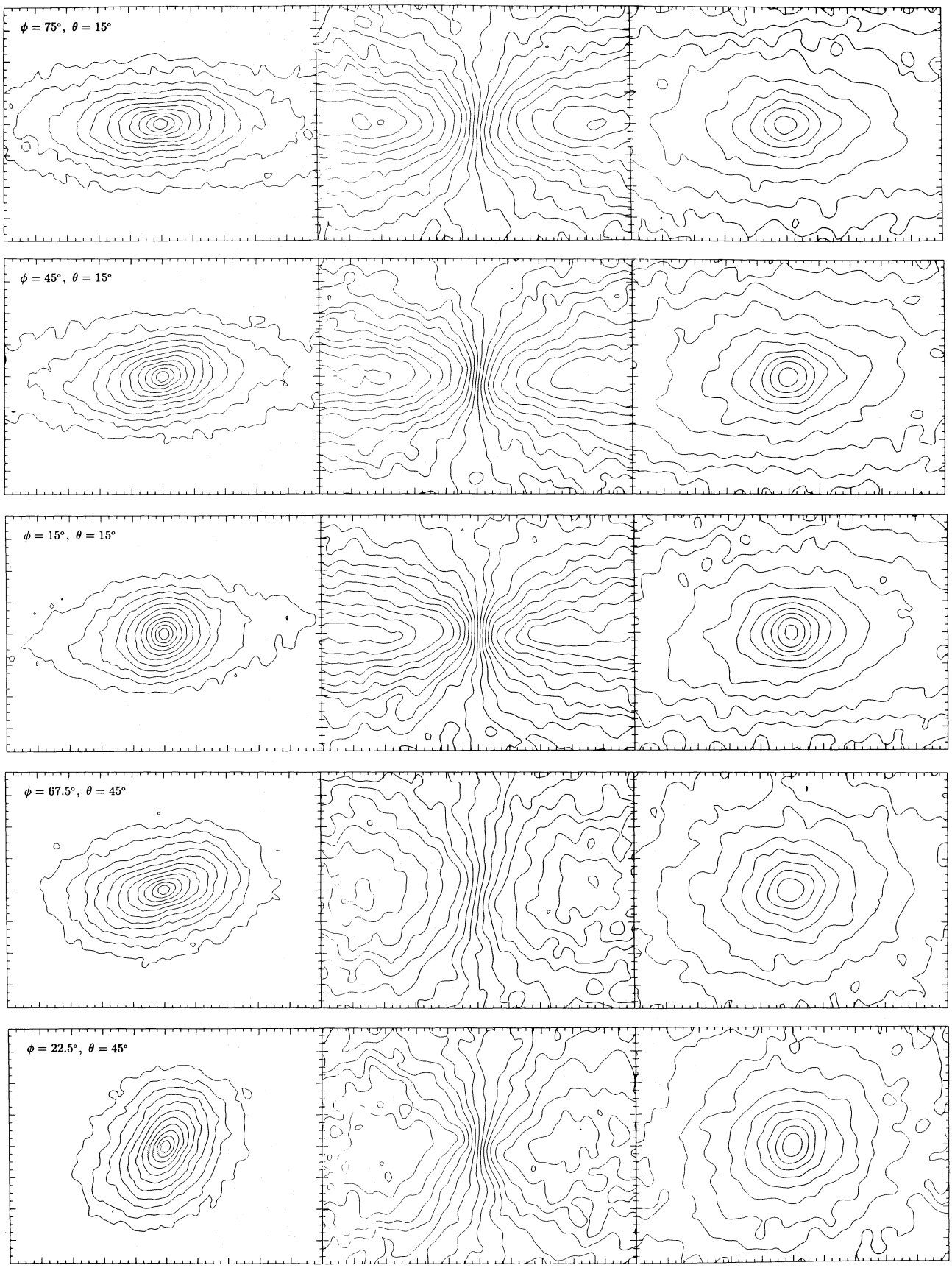

Fig. 6. (continued) The contour levels are at half-magnitude intervals for the density, at 0.02 ($\approx$ 20 km/s) for the radial velocity ($V_{\rm rad}$: ... $-0.03, -0.01, 0.01, 0.03, \ldots$) and velocity dispersion ($\sigma_{\rm rad}$: $0.02, 0.04, \ldots$). The interval between large ticks corresponds to 2 kpc.

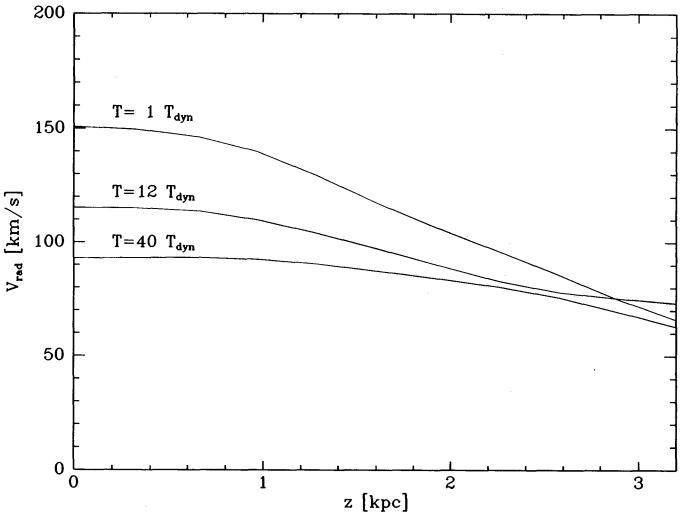

Fig. 7. Projected radial velocity as a function of z at $R=3$ kpc in model N, at $T=1$, 12 and 40 $T_{\rm dyn}$.

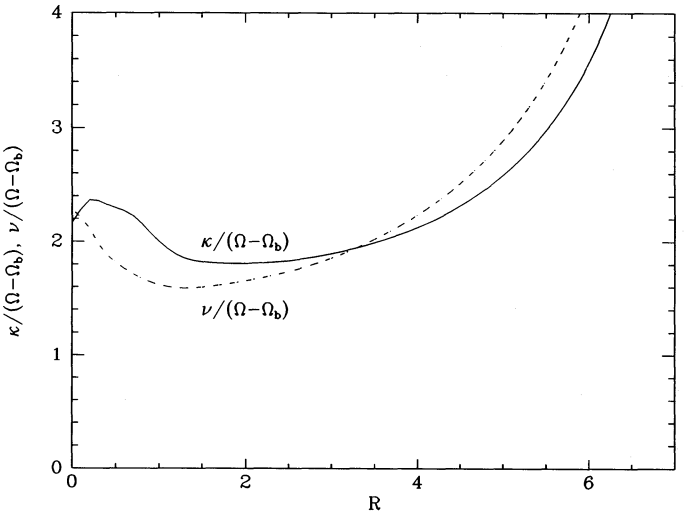

Fig. 8. Resonance diagram: axisymmetric frequency ratios $\kappa/(\Omega-\Omega_b)$, $\nu_z/(\Omega-\Omega_b)$ as a function of R (run O at $T=20\,T_{\rm dyn}$).

that these axisymmetric resonances are real by considering the periodic orbits in the bar. More detail will be provided in other papers.

A remarkable fact is that the position of the maximum elevation above the plane, the peanut swell, corresponds to the radius of both the axisymmetric horizontal and vertical inner Lindblad resonance (ILR): $\Omega_b=\Omega-\kappa/2$ and $\Omega_b=\Omega-\nu_z/2$, therefore $\kappa=\nu_z$. In all cases Ω_b is close to the maximum of the curve $\Omega-\kappa/2$ (Fig. 8), but the direct families x_2 or x_3 perpendicular to the bar have either a very small extent, or more frequently do not exist at all. Therefore, the radius of the swell of the peanut is essentially determined by the vertical ILR, which has a very limited extension in phase-space. At this radius $\kappa\approx\nu_z$.

3.8. Orbit frequencies

As another check of the actual frequencies of the stars, we have counted (in the N-body simulations) the number of rotations,

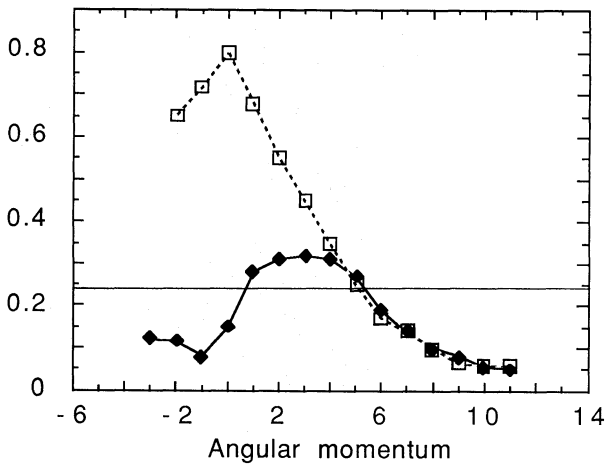

Fig. 9. Average values of $\Omega-\kappa/2$ (filled diamonds) and $\Omega-\nu_z/2$ (open squares) obtained from the actual frequencies of the particles, as a function of the specific angular momentum, for the run B. The horizontal line corresponds to the bar rotation frequency Ω_b.

the number of radial epicycles and z-oscillations performed by each particle, during several rotations of the bar, when it has reached a steady state.

The average values of $\Omega-\kappa/2$ and $\Omega-\nu_z/2$ are plotted as a function of the average specific angular momentum in Fig. 9. This plot reveals that a significant number of particles in the disk are resonant (or nearly resonant) with the bar, and that the two ILR's (horizontal and vertical) influence the same range of angular momentum (i.e. mean radii). Of course, the fact that orbits are nearly resonant is not sufficient for implying the existence of the corresponding resonance.

3.9. Orbits making the peanut

By examining either the stable periodic orbits in the frozen bar potential rotating at a constant speed, or by examining the motion of randomly chosen particles in the N-body simulations, the orbits supporting the peanut shape can be revealed.

Examples of periodic and quasi-periodic orbits supporting the peanut is shown in Fig. 10. They consist of orbits elongated along the bar, with frequency ratios $\Omega/\kappa/\nu_z=1/2/2$.

As well known, the concepts of eigen-frequencies and actions are well defined for regular orbits only. But not all the orbits are regular, indeed numerous chaotic orbits starting in the same region of phase space, exhibiting semi-ergodic behaviour, are also present and are another typical effect of resonances. An essential ingredient necessary for producing peanut shapes is that the orbits supporting it exist only over a sharply delimited range outwards. Indeed, at larger radii or energy, the quasi-periodic orbits supported by the 1/2/2 periodic orbits stop suddenly to exist and are replaced by more chaotic orbits produced by the corotation resonance and higher order resonances (Fig. 10, bottom).

4. Discussion

Our N-body simulations reveal the presence of a peanut shape in all galaxy disks which have developed a strong bar. This phenomenon gets a better understanding by comparing the

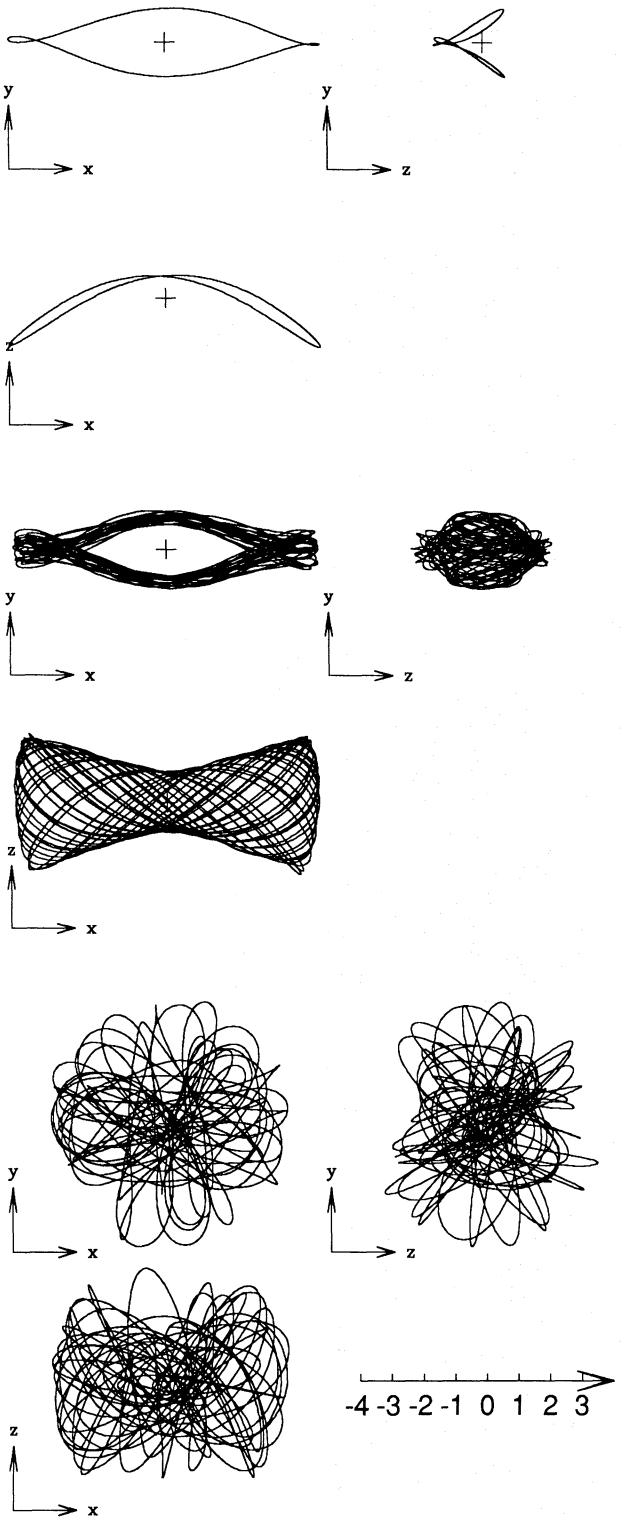

Fig. 10. Regular orbits supporting the peanut shape: top, 3-D periodic orbit, middle 3-D quasi-periodic orbit. Bottom, a 3-D chaotic orbit starting in a nearby region of phase space (run O at $T = 20\, T_{\mathrm{dyn}}$).

macroscopic features of the bar dynamic (such as resonances) with the microscopic ones (such as the periodic orbits and their bifurcations).

The swell of the peanut is made up by stars trapped in the bar, since the disk beyond the bar has not thickened, and a hot bulge is rather insensitive even to the formation of the bar. This is easily seen on an edge-on projection of the density, when the bar is end-on (Fig. 6, $\phi = 0°$, $\theta = 0°$). There is no kind of torus generated at the radius of maximum elevation above the plane. The majority of stars forming such a bar are elongated orbits precessing about the center at a common rate $\Omega - \kappa/2 \approx \Omega_b$, where the effective epicyclic rate κ, and as well as the effective ν_z, are slightly different in the strong bar deformation than in an axisymmetric averaged mass distribution. At some distance from the center, about midway from the corotation radius, the two oscillation rates κ and ν_z are comparable. Numerous resonant (or nearly-resonant) orbits with the characteristic frequencies Ω, $\Omega - \nu_z/2$, and $\Omega - \kappa/2$ are indeed found (Fig. 10).

Deeper studies of this resonance on stars orbits are underway; some of the results already presented in Sect. 3.9 shed light on the conclusions obtained from the N-body codes. This frequency locking between horizontal and vertical oscillations is the basic reason for an approximate cylindrical rotation, because stars with large excursions in z have nevertheless to follow the bar, their average speed can not be much different from the bar speed. Therefore, the bar is more intimately linked to the cylindrical rotation than the box shape is. Contrary to a rotating bar, it is indeed conceivable to build an axisymmetric box-shaped figure without rotation, or cylindrical rotation, since in such a case the amount of retrograde motion can be chosen arbitrary.

The resonances found are not necessarily the unique ones which could produce a boxy bulge. One could imagine for instance that a flat bar (with axis ratios such as 1 : 0.25 : 0.10, recommended by observers, e.g. Kormendy, 1982), would produce large values of ν_z, and the bar-bulge could be locked for instance by a $\Omega - \nu_z/4$ vertical resonance (ultra-harmonic resonance). Stable 1/4/4 orbits in such a flat bar had been found in earlier works (Pfenniger, 1984, 1985) to take also a boxy shape, with dimensions similar to the ones of the 1/2/2 orbits described here. However, the higher the resonance order is, the smaller is its width typically. Therefore, the probability to be trapped by such a higher order resonance is a priori lesser than by the low order ones that we obtain. A factor which could somewhat penalize the development of high order resonances, which need flatter mass distribution than the low order ones, is the finite resolution of the grid. The softening of the potential limits the short range correlations between the particles, but it does not prevent orbits to be affected by orbital resonances. Since typical 1/4/4 orbits have z-extension comparable to the 1/2/2 orbits, it is unlikely that softening alone is responsible for the systematic apparition of the 1/2/2 orbits.

So a discrepancy still remains between what the observers (e.g. Kormendy, 1982) believe about the flatness of real bars, and the bars produced by the simulations. A possible reason could be that when a bar builds up, starting from a flat partly gaseous disk, it would be indeed very flat for some rotation periods and more easily identified as a bar when seen edge-on. But, in a few dynamical times, the bar would be diluted in z by vertical instabilities, and then its barred nature would be much less obvious when seen edge-on. By rotating and projecting the models, we find that it is indeed very difficult to guess a bar from many edge-on projection angles. We point out also that the fraction of bars detected with confidence in edge-on galaxies is much lower than in face-on galaxies. Necessarily, many edge-on galaxies are barred but look like non-barred galaxies.

N-body simulations show that tidal galaxy interactions destroy often rapidly the axisymmetry of disks, and easily trigger the

formation of a bar (Noguchi, 1987; Gérin, Combes & Athanassoula, 1989), especially if the Q parameter is not far from critical. So, the formation of a box- or peanut-shaped galaxy can also be induced indirectly by some collisional process: the perturber triggers or accelerates the formation of a bar, which, on a longer time-scale, can then produce the boxiness by means of the same resonance process as discussed above.

We notice that squarish shapes analogous to the stellar dynamical peanut shapes are also obtained in models of rapidly rotating gaseous bodies (e.g. Stoeckly, 1965; Bodenheimer & Ostriker, 1973), but that too rapidly rotating gaseous axisymmetric bodies are also bar unstable (e.g. Durisen et al., 1986). Therefore, this analogy suggests that the primordial cause of peanut shape is a fast rotation, and if this rotation is large enough, at some critical point a triaxial boxy figure is unavoidable. The N-body model of May et al. (1985) is box-shaped but axisymmetric, so it rotates slowly enough and is hot enough for being bar stable, while N-body models such as those of Hohl & Zang (1979), Miller & Smith (1979), Combes & Sanders (1981) or those of this study rotate fast enough for preferring the bar shape.

5. Conclusions

We have shown that every stellar bar produced in our model galaxies takes a final box-peanut morphology, whatever the bulge-to-disk mass ratio or radial scales are. The fact that the box-peanut develops with a certain delay after the bar formation, and that the swelling of the plane is not axisymmetric, but occurs only along the bar (as a real 3-D peanut), strongly suggests a resonance mechanism: the stars making up the peanut are resonant with the bar. The inflated zone of the peanut corresponds to the horizontal ILR $\Omega_b = \Omega - \kappa/2$, and also to its vertical analog $\Omega_b = \Omega - \nu_z/2$. The conjunction of these two resonances enhances their effect, and explains why there is no torus but a peanut. For all our model galaxies, the two resonances coincide at the end of the run, when the bar is in a steady state, resulting from a self-adjustment of the density distribution. As the evolution proceeds, the surface density of the disk becomes exponential, the scale-height of the disk increases in the bar region, such that $\kappa \approx \nu_z$ at the maximum height of the peanut, and the angular velocity of the bar decreases until $\Omega_b \approx \Omega - \kappa/2$. Since the bar ends at about its corotation radius, a marginal horizontal ILR and a vertical ILR occur just midway between the center and the bar end.

Various projections of a box-peanut-shaped bar, the corresponding isophotes and kinematics have been compared with observations. The morphology and the cylindrical rotation agree fairly well with the analogs observed by Jarvis (1990) in NGC 128, the prototype of peanut-galaxies. Provided that nothing destroys the bars before, as perhaps dissipational effects enhancing a central mass concentration (Pfenniger & Norman, 1990), we predict that all barred galaxies will take box and peanut shapes when viewed edge-on. The actual fraction of boxy bulges of edge-on spirals is observed to be around 20% (Jarvis, 1986; Shaw, 1987, 1989; de Souza & dos Anjos, 1987; Dettmar, 1989). So, taking into account that the time-scale necessary for the development of the box after the bar formation amounts typically to ten rotation periods, and that not all projection angles are favorable to their detection, this percentage is consistent with the interpretation that all observed box- or peanut-shaped bulges are strong bars, since the fraction of face-on strong bars (SB type) amounts to about 30%.

In summary, we propose that perhaps all, but at least a substantial fraction of box and peanut disk galaxies are barred, and that the bar is the generator of these peculiar morphologies. Some boxy ellipticals can also be relevant to this scheme, when high cylindrical rotation is detected, but this might be only marginal, and might concern only misclassified lenticulars among disk-ellipticals. As for the boxy ellipticals which have no significant disk, there must be another mechanism to account for their distortion.

Acknowledgements. This work has benefited of the continuous interest of Prof. L. Martinet and of useful discussions with James Binney, Brian Jarvis and Martin Shaw. It has been supported by the University of Geneva (Geneva Observatory), the Swiss National Science Foundation, and the Institute for Advanced Study. Part of the calculations have been done on the CRAY-2 of the CCVR, "Centre de Calcul Vectoriel pour la Recherche", in the Ecole Polytechnique, Palaiseau (France), and on the CRAY-2 of the Ecole Polytechnique Fédérale in Lausanne.

References

Bailey, M.E., Wilkinson, A.: 1990, in preparation
Bender, R., Möllenhoff, C.: 1987, *Astron. Astrophys.* **177,** 71
Bertola, F., Capaccioli, M.: 1977, *Astrophys. J.* **211,** 697
Binney, J.: 1982, *Ann. Rev. Astron. Astrophys.* **20,** 399
Binney, J., Petrou, M.: 1985, *Monthly Notices Roy. Astron. Soc.* **214,** 449
Bodenheimer, P., Ostriker, J.P.: 1973, *Astrophys. J.* **180,** 159
Buneman, O.: 1967, *J. Comp. Phys.* **1,** 517
Burbidge, E.M., Burbidge, G.R.: 1959, *Astrophys. J.* **130,** 20
Combes, F., Sanders, R.H.: 1981, *Astron. Astrophys.* **96,** 164 (CS)
Debbasch, F., Combes, F.: 1990, *Astron. Astrophys.* in preparation
de Carvalho, R.R., da Costa, L.N.: 1987, *Astron. Astrophys.* **171,** 66
de Souza, R.E., dos Anjos, S.: 1987, *Astron. Astrophys. Suppl.* **70,** 465
Dettmar, R.J.: 1989, in *The World of Galaxies,* Proceedings of the Conference "Le Monde des Galaxies", eds. H.G. Corwin, L. Bottinelli, Springer, New-York, p. 229
Dettmar, R.J., Barteldrees, A.: 1988, *173rd AAS Meeting,* **20,** No 4, 1085
Durisen, R.H., Gingold, R.A., Tohline, J.E., Boss, A.P.: 1986, *Astrophys. J.* **305,** 281
Gérin, M., Combes, F., Athanassoula, E.: 1989, *Astron. Astrophys.,* in press
Hockney, R.W., Eastwood, J.W.: 1981, in *Computer Simulation Using Particles,* McGraw-Hill
Hohl, F.: 1971, *Astrophys. J.* **168,** 343
Hohl, F., Zang, T.A.: 1979, *Astron. J.* **84,** 585
Jarvis, B.J.: 1986, *Astron. J.* **91,** 65
Jarvis, B.J.: 1987, *Astron. J.* **94,** 30
Jarvis, B.J.: 1990, *Heidelberg Conference on the Dynamics and Interactions of Galaxies,* ed. R. Wielen, Springer, in press
Jedrzejewski, R.I.: 1987, *Monthly Notices Roy. Astron. Soc.* **226,** 747

Jensen, E., Thuan, T.X.: 1982, *Astrophys. J. Suppl.* **50,** 421
Kormendy, J.: 1982, in *Morphology and Dynamics of Galaxies,* Saas-Fee Twelfth Advanced Course of the Swiss Society of Astronomy and Astrophysics, eds. L. Martinet, M. Mayor, Geneva Observatory, Geneva, p. 113
Kormendy, J., Illingworth, G.: 1982, *Astrophys. J.* **256,** 460
Kuzmin, G.: 1956, *Astrophys. Zh.* **33,** 27
Lauer, T.R.: 1985a, *Astrophys. J. Suppl.* **57,** 473
Lauer, T.R.: 1985b, *Monthly Notices Roy. Astron. Soc.* **216,** 429
May, A., van Albada, T.S., Norman, C.A.: 1985, *Monthly Notices Roy. Astron. Soc.* **214,** 131
Miller, R.H.: 1976, *J. Comp. Phys.* **21,** 400
Miller, R.H.: 1978, *Astrophys. J.* **223,** 811
Miller, R.H., Smith, B.F.: 1979, *Astrophys. J.* **227,** 785
Miyamoto, M., Nagai, R.: 1975, *Publ. Astron. Soc. Japan* **27,** 533
Nagai, R., Miyamoto, M.: 1976, *Publ. Astron. Soc. Japan* **28,** 1
Nieto, J.-L.: 1988, in *Second Extragalactic Astronomy Regional Meeting,* Cordoba, Argentina, p. 239
Noguchi, M.: 1987, *Monthly Notices Roy. Astron. Soc.* **228,** 635
Petrou, M.: 1987, *Monthly Notices Roy. Astron. Soc.* **226,** 111
Pfenniger, D.: 1984, *Astron. Astrophys.* **134,** 373
Pfenniger, D.: 1985, *Astron. Astrophys.* **150,** 112
Pfenniger, D., Friedli, D.: 1990, *Astron. Astrophys.* in preparation
Pfenniger, D., Norman, C.: 1990, *Astrophys. J.* submitted
Rowley, G.: 1988, *Astrophys. J.* **331,** 124
Sandage, A.: 1961, *The Hubble Atlas of Galaxies,* Carnegie Inst. of Washington, Washington, D.C.
Schweizer, F.: 1986, in *Structure and Dynamics of Elliptical Galaxies,* I.A.U. Symp. No. 127, ed. T. de Zeeuw, Reidel, Dordrecht, p. 109
Sellwood, J.A.: 1980, *Astron. Astrophys.* **89,** 296
Sellwood, J.A.: 1981, *Astron. Astrophys.* **99,** 362
Sellwood, J.A.: 1987, *Ann. Rev. Astron. Astrophys.* **25,** 151
Shaw, M.: 1987, *Monthly Notices Roy. Astron. Soc.* **229,** 691
Shaw, M.: 1989, in *The World of Galaxies,* Proceedings of the Conference "Le Monde des Galaxies", eds. H.G. Corwin, L. Bottinelli, Springer, New-York, p. 235
Stoeckly, R.: 1965, *Astrophys. J.* **152,** 208
Toomre, A.: 1964, *Astrophys. J.* **139,** 1217
Toomre, A.: 1977, in *The Evolution of Galaxies and Stellar Populations,* eds. B.M. Tinsley & R.B. Larson, Yale University, New Haven, p. 401
Weinberg, M.D.: 1985, *Monthly Notices Roy. Astron. Soc.* **213,** 451
Whitmore, B.C., Bell M.: 1988, *Astrophys. J.* **324,** 741

This article was processed by the authors using Springer-Verlag TEX AA macro package 1989.